



# Development of damage curves for buildings near La Rochelle during Storm Xynthia based on insurance claims and hydrodynamic simulations

Manuel Andres Diaz Loaiza<sup>1</sup>, Jeremy David Bricker<sup>1,4</sup>, Remi Meynadier<sup>2</sup>, Trang Duong<sup>3</sup>, Rosh Ranasinghe<sup>3</sup> and Sebastiaan Nicolaas Jonkman<sup>1</sup>

<sup>1</sup>Department of Hydraulic Engineering, Delft University of Technology, Delft, The Netherlands

<sup>2</sup>AXA Insurance, Group Risk Management, Paris, France

<sup>3</sup>IHE Delft, Institute for Water Education, Department of Water Science and Engineering, Delft, The Netherlands

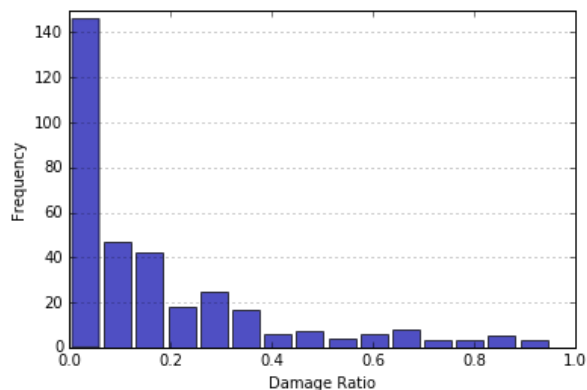
<sup>4</sup>Department of Civil & Environmental Engineering, University of Michigan, Ann Arbor, MI, USA

10 *Correspondence to:* Jeremy Bricker (j.d.bricker@tudelft.nl)

**Abstract.** The Delft3D hydrodynamic and wave model is used to hindcast the storm surge and waves that impacted La Rochelle, France and the surrounding area (Aytré, Châtelaillon-Plage, Yves, Fouras and Ille du Re) during Storm Xynthia. These models are validated against tide and wave measurements. The models then estimate the footprint of flow depth, speed, unit discharge, flow momentum flux, significant wave height, wave energy flux, total water depth (flow depth plus wave height), and total (flow plus wave) force at the locations of damaged buildings for which insurance claims data are available. Correlation of the hydrodynamic and wave results with the claims data generates building damage functions. These damage functions are shown to be sensitive to the topography data used in the simulation, as well as the hydrodynamic or wave forcing parameter chosen for the correlation. The most robust damage functions result from highly accurate topographic data, and are correlated with water depth or total (flow plus wave) force.

## 20 1 Introduction

In 2010 the Xynthia extratropical storm caused damage to the Atlantic coast of Spain and France (Slomp et al., 2010, Chauveau et al. 2011). The present paper develops damage curves for buildings in the area where the storm surge and waves of Xynthia storm caused the most damage. We draw methods used to quantify damage due to hurricanes and tsunamis in the USA and Japan (Suppasri 2013, Hatzikyriakou et al., 2018, Tomiczek et al., 2017), but for the first time apply these to modern masonry structures in Europe affected by storm surge and waves from an extratropical cyclone. A total of 423 reported claims in the area of study were used (Figure 1). The damage ratio (DR) is defined as the ratio of damages claimed by each property, to the total insured value of that property. More than 9% of the structures had a damage ratio (DR) higher than 0.5 (considerable damages), 30% had DR higher than 0.2 (medium damages) and 49% had low damages.



30

**Figure 1: Damage ratio histogram for insurance claims data in the region.**

The damage curve is an important tool in risk assessment science related to the vulnerability of structures (Pistrika et al., 2010; Enghardt et al., 2019). From the structural point of view, damage curves depend on the construction materials that buildings are made of (Huizinga, et al., 2017; Postacchini et al., 2019). Damage curves also depend on construction methods, codes, and building layout, including the distance between buildings (Suppasri et al., 2013; Jansen et al., 2020). The current paper focuses on 1-2 story masonry buildings under the effect of storm surge and wave forces produced by an extratropical storm in northwest France. The Xynthia storm provided a rare dataset of empirical measured damage from coastal flooding in a European country.

35

## 2 Methods

As shown schematically in Figure 2, Delft3D-FLOW calculates non-steady flow phenomena that result from tidal and meteorological forcing on a rectilinear or a curvilinear grid (Deltares, 2021). At the same time, and coupled with Delft3d, a numerical wave model (SWAN) calculates significant wave height and period fields. Delft3D-FLOW and SWAN were used to hindcast the physical forcing at the locations of all claims in the database. Afterwards, a probability standardized normal distribution function proposed by Suppasri et al., 2013 was used to develop damage curves by correlating claimed damage with a variety of hydrodynamic forcing variables.

45

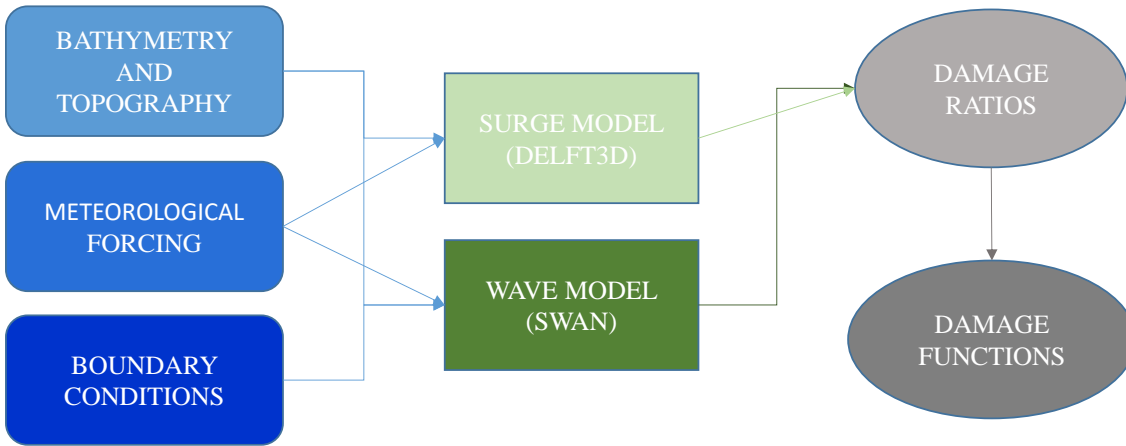


**Figure 2: Flow chart of the framework used in development of damage curves.**

Damage curves are commonly developed by the correlation of field or laboratory measurements of damage, with numerical simulations of hazard level. Tsubaki et al. (2016) measured railway embankment and ballast scour in the field, and correlated this damage with flood overflow surcharge calculated by a hydrodynamic flood simulation. Englhardt et al. (2019) and Huizinga et al. (2017) used big-data analytics to correlate tabulated damages with estimated flood levels over a large scale. Pregnotato et al. (2015) showed that most damage functions are based on flood depth alone, though a few also consider flow speed (De Risi et al., 2017; Jansen et al., 2020) or flood duration. The water depth is an important variable since it accounts for the static forces that act over a structure. Nevertheless, in storm events, structures close to the coast at a foreshore/backshore can be subjected to dynamical forces like the action of flow and waves (Kreibich et al., 2009; Tomiczek et al., 2017). For this reason, In order to consider other possible forces the following hydrodynamic parameters are analysed: water depth ( $h$ ), flow speed ( $v$ ), unit discharge ( $hv$ ), flow momentum flux ( $\rho hv^2$ ), significant wave height ( $H_{sig}$ ), total water depth ( $h + H_{sig}$ ), wave energy flux ( $E_f$ ), and total force ( $\frac{E_f}{C_g} + \rho hv^2$ ). The wave energy flux is defined via Eq. (1) as in Bricker J. et al., 2017:

$$E_f = \frac{1}{16} \rho g H_{sig}^2 C_g, \quad (1)$$

where  $H_{sig}$  is the significant wave height,  $C_g$  is the wave group velocity,  $\rho$  is the water density and  $g$  is the acceleration due to gravity, and  $C_g = \sqrt{gh}$  over land where waves impact buildings.

### 2.1 Hydrodynamic model of the Xynthia Storm

In order to capture the hydrodynamic storm characteristics a regional model domain over the Atlantic Spanish and French coasts was built. Domain decomposition was implemented with grids of resolution of ~2km over the open ocean, ~400m close to the study area and ~80m over the area of claims data (Figure 23).

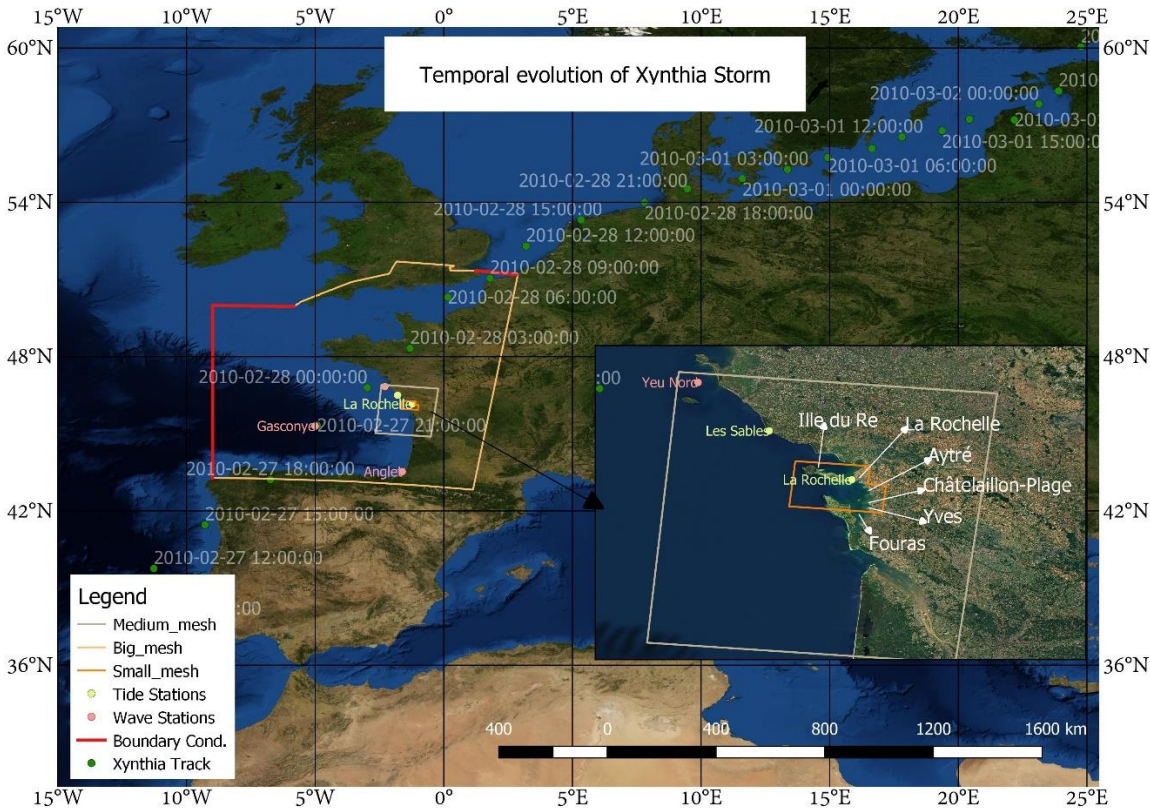


**Figure 3: Domain decomposition of three nested grids running in parallel. The Xynthia storm track is shown with minimum atmospheric pressure of 966 hPa at 2010-02-27 21:00:00 (Extreme Wind Storm Catalogue). Satellite image by OpenLayers – QGIS.**

### 70 2.1.1 Topography and Bathymetry

We use two types of topography datasets: a global dataset for the bathymetry/topography (GEBCO 2019, which is based on SRTM 15+ v2 over land), and a higher resolution bathymetry (MNT – HOMONIM project) and topography (IGN institute). Luppichini et al. (2019) and Ettritcha et al. (2018) found that the quality of bathymetry and topography data has a large effect on estimation of the hazard, and Brussee et al. (2021) similarly found topography data quality affects resulting damage estimates. In order to investigate the effect of the quality of topographic and bathymetric data on the resulting damage functions, three scenarios are considered in our work (Table 1).

**Table 1: Case studies for investigating sensitivity of model result to DEM resolution.**

Item	Low resolution (a)	High resolution (b)	High resolution + structures (c)
Topography	GEBCO (500m)	IGN (5m)	IGN (5m) + flood walls surveyed by the authors with an RTK-GPS



Bathymetry	GEBCO (500m)	GEBCO (500m) in deep water + MNT (100m) nearshore	GEBCO (500m) in deep water + MNT (100m) nearshore
------------	--------------	---	---

## 80 2.1.2 Meteorological setup

To generate pressure and wind fields to drive the storm surge model, dynamically downscaled surface meteorological data were generated for the French Atlantic study region (Figure 3). It contains zonal and meridional winds 10 m above ground ( $u_{10}, v_{10}$ ) and surface pressures over sea and land, with 3.5 km spatial resolution and temporal every 3hrs. The dynamical downscaling was performed with the regional climate model WRF (Skamarock et al., 2008), based on NCEP CFSR reanalysis data (Saha et al., 2010). The regional non-hydrostatic WRF model (version 3.4) simulated 15 February 2010 until 05 March 2010. The initial and lateral boundary conditions are taken from the CFSR reanalysis at 0.5° resolution, updated every 6 h. The horizontal resolution is 7 km; we use a vertical resolution of 35 sigma levels with a top-of-atmosphere at 50hPa. The simulation domain was chosen to be wide enough in latitude and longitude for WRF to fully simulate the large-scale atmospheric features of the Xynthia extratropical cyclone. A spin-up time of 5 days was considered in the study to remove spurious effects of the top layer soil moisture adjustment even though most of the analyses here are performed over the ocean. Land surface processes are resolved by using the Noah Land Surface Model scheme with four soil layers. Numerical schemes used in the Xynthia downscaling WRF simulation are the Multi-Scale Kain-Fritsch scheme for convection, the Yonsei University scheme for the planetary boundary layer, the WRF Single-Moment 6-class scheme for microphysics, and the RRTMG scheme for shortwave and longwave radiation. WRF outputs are generated every 3 hours.

## 95 2.2 Hydrodynamic and Wave Model setup

Delft3d was coupled together with SWAN in a domain decomposition mode in order to hindcast storm tide and waves. Model boundary conditions consisted of astronomical tidal water elevations from the Global Tide and Surge Model (GTSM) of Muis et al. (2016) for the period from 20 February until 1 March 2010. The hydrodynamic model was run with a computational time step of 30 sec and a uniform Manning's n of 0.025. The air-sea drag coefficient of Smith and Banke (1975) was used. Other model parameters retained their default settings.

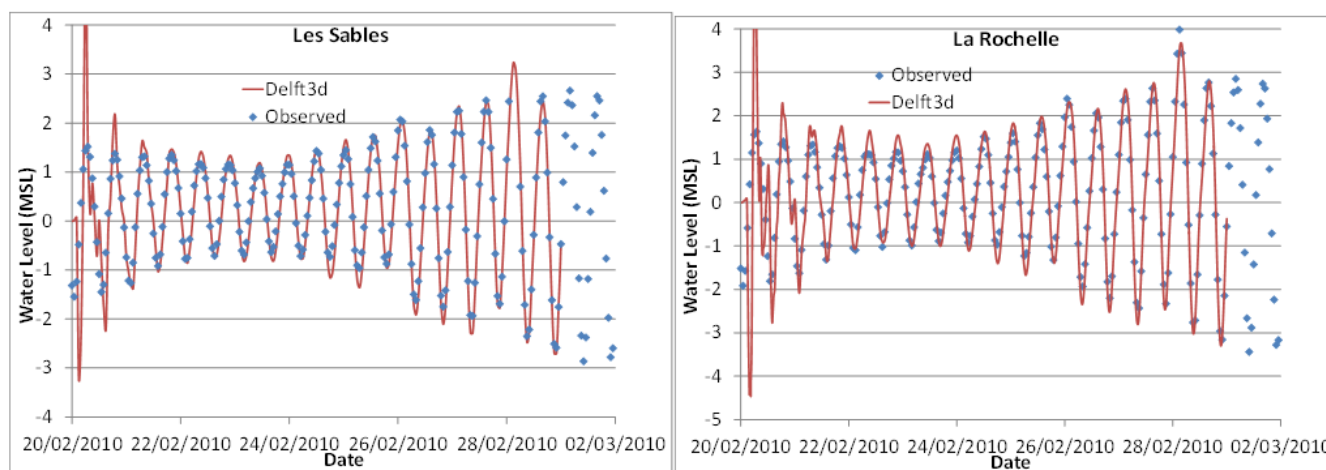
## 2.3 Hydrodynamic and wave model validation

### 2.3.1 Storm tide validation

The hydrodynamic model was run from 20 February until 1 March 2010, the duration of the meteorological forcing data, with GTSM astronomical tide boundary conditions. After 2 days of model spin-up, the comparison between the observed water levels from SHOM tide gauges, and modelled water levels from Delft3d, during the whole simulation is good (Figure 4). Note



that the Les Sables gauge failed at the peak of the storm (on 2010-02-28 03:00:00) so a data point is missing in the observations at that time. At La Rochelle the difference between the observed and modelled is only 36cm at peak storm tide.



110 **Figure 4: Observed and modelled tide at La Rochelle and Les Sables. Note that during the peak of the storm tide at Les Sables, the tide measuring gauge was out of operation, resulting in a missing data point in that data series.**

### 2.3.2 Wave model validation

The wave model was validated against data from the CORIOLIS operational oceanography center (<http://www.coriolis.eu.org/About-Coriolis>) in Figure 5.

115

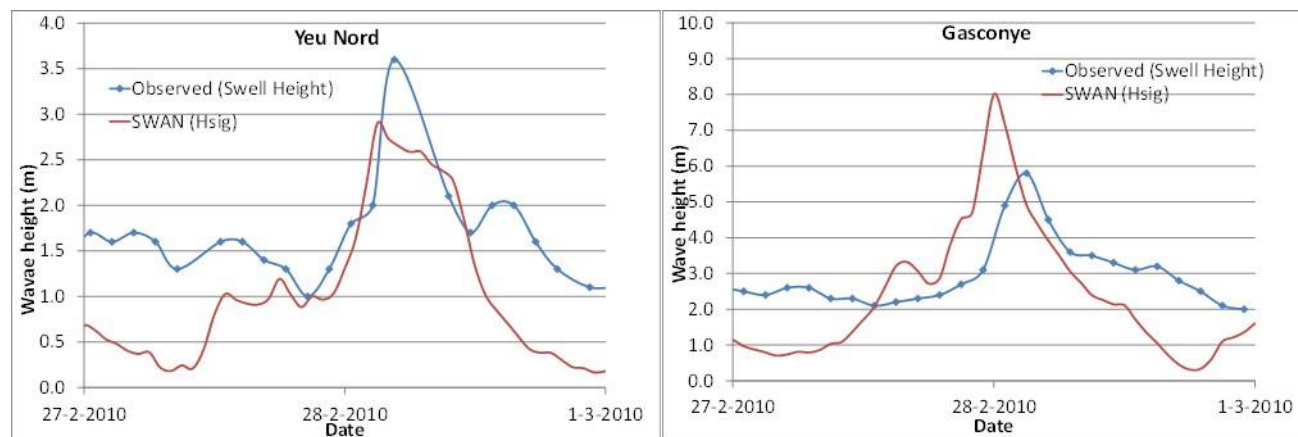


**Figure 5: Deep water buoys of Yeu Nord (left) and Gasconye (right). In the first case the buoy is located close by an Island with the same name. The second is located in open ocean almost in the middle of the Viscay gulf.**



## 2.4 Damage curves

120 Damage curves express the amount of damage experienced by a structure, relative to the structure's total insured value. More specifically, relates the cumulative distribution function, usually in terms of the standardized normal distribution function with the damages (Suppasri et al., 2013; Sihombing and Torbol, 2016).

$$P(x) = \Phi \left[ \frac{x-\mu}{\sigma} \right], \quad (2)$$

where  $P(x)$  is the cumulative probability of damage level  $x$ ,  $\Phi$  is the standardized normal distribution,  $\mu$  is the median and  $\sigma$  the standard deviation (Tsubaki et al., 2016). It is also very common to express the previous equation as a logarithmic function in order to obtain easily the parameters of the distribution with least square fitting as proposed by Suppasri et al., 2013. In the present paper the parameters are assessed using the L-moments package within the open source program R. In this way it is possible to relate different hydrodynamic variables with the damage ratio. From the 423 claims data within our domain, approximately 185 are on Ille du Re, and the remaining 238 in the towns of La Rochelle, Aytré, Yves, Châtelailon-Plage and Fouras.

## 3 Results

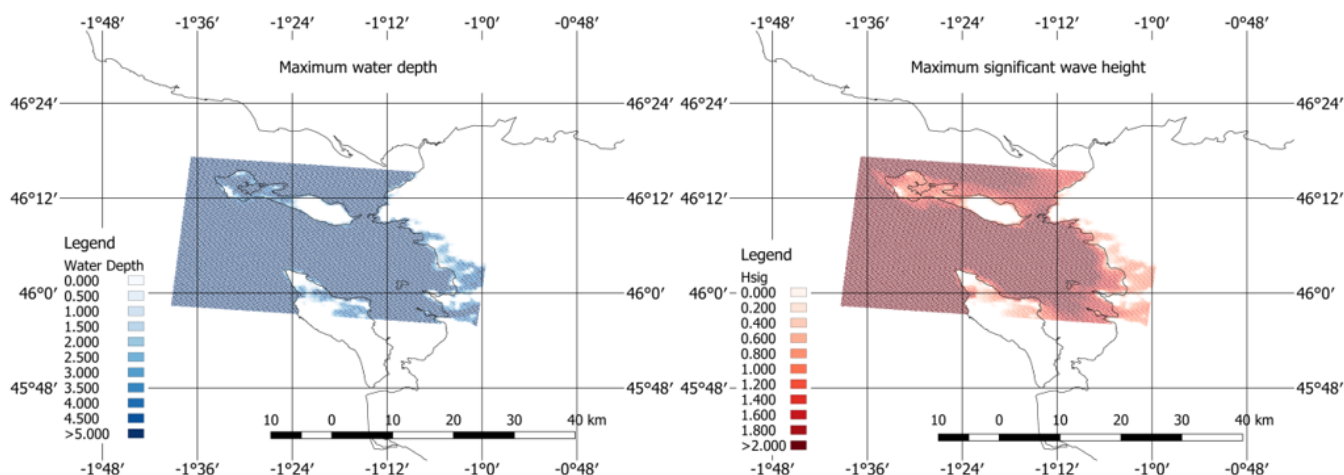
After determining the model hydrodynamic and wave results (Figure 6) at the location of each claim location, the data were subdivided into ten categories according to damage ratio level, and Box-Whisker plots were built to display the entire dataset and analyse the trend of the data (Appendix A). Among the flow-only variables, the unit discharge ( $hv$ ) appears to have the clearest trend and least scatter. From the variables related to both flow and waves, the total force ( $\frac{E_f}{C_g} + \rho hv^2$ ) appears to have the clearest trend and correlation with the damage ratio. To better understand which of the variables fit Damage functions best, three accuracy indicators are assessed: root mean square error (RMSE, Equation 3), Relative root square error (RRSE, Equation 4), and the Pearson correlation coefficient ( $\rho$ , Equation 5).

$$RMSE = \sqrt{\frac{\sum_1^T (y' - y)^2}{T}}, \quad (3)$$

$$140 \quad RRSE = \sqrt{\frac{\sum_1^T (y' - y)^2}{\sum_1^T (y - \bar{y})^2}}, \quad \bar{y} = \frac{\sum_1^T y}{T} \quad (4)$$

$$\rho_{y,y'} = \frac{cov(y,y')}{\sigma_y \sigma_{y'}}, \quad (5)$$

Where  $y'$  is the predicted value,  $y$  is the actual value and  $\bar{y}$  is the average of the actual values to predict,  $T$  is the number of values, and  $\sigma$  indicate the standard deviation



145 **Figure 6: Maximum water level and maximum significant wave height footprints for the finer domain (case study area). water depth and wave height are in units of m.**

### 3.4 Damage curves from each digital elevation model

In order to build the damage curves with equation (2), the median values are extracted from the boxplots of appendix A (figures A1 to A3) for each variable. In Figure 7 the damage curves for each hydrodynamic parameter are displayed in 3 lines, one for each digital elevation model of Table 1. Similarly to Reese and Ramsay (2010), we find that greater than 90% of damage  
150 occurs in the first 5m of flood depth.



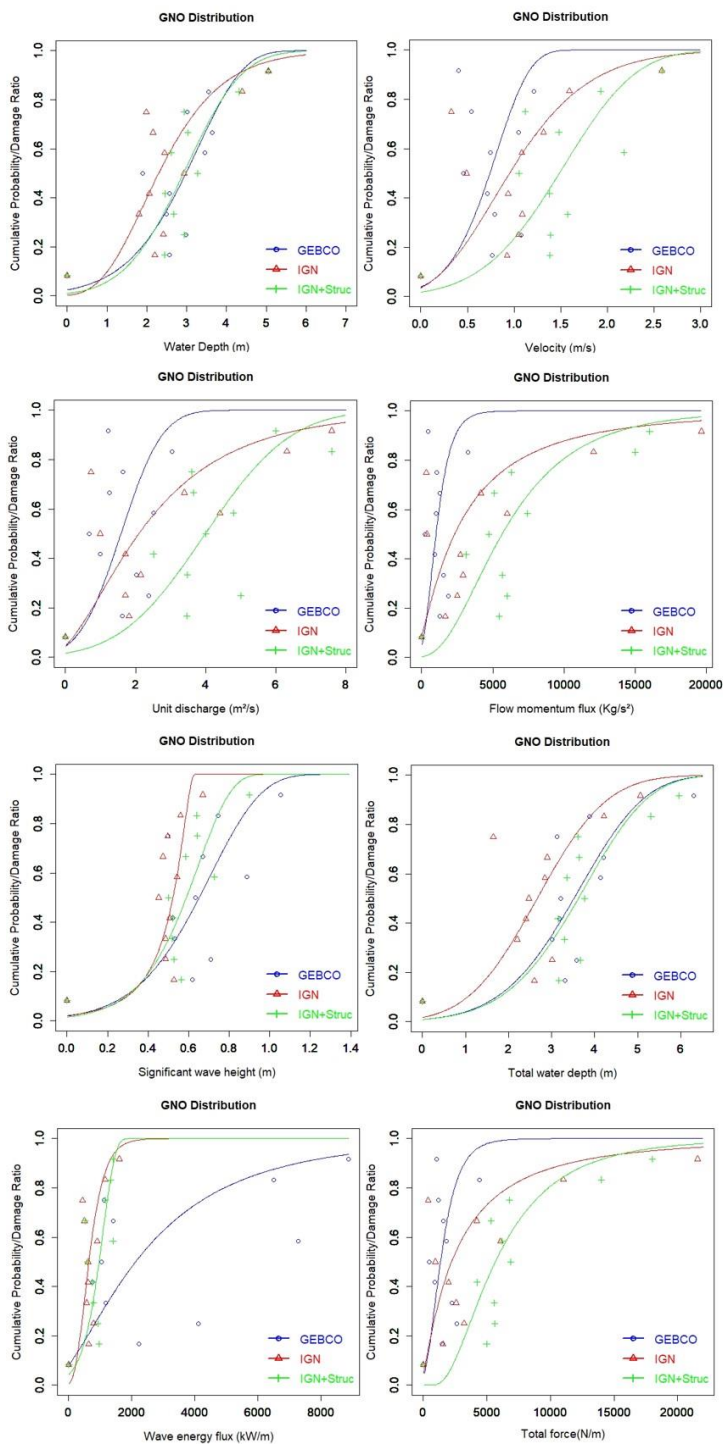


Figure 7: Damage curves for the surge and wave variables ( $h$ ,  $v$ ,  $hv$ ,  $hv^2$ ,  $H_{sig}$ ,  $h + H_{sig}$ ,  $E_f$ ,  $\frac{E_f}{C_g} + \rho hv^2$ ).



155 Table 2 shows that among the hydrodynamic parameters related only to storm surge, the water depth best fits Equation (2), with the lowest errors (RMSE and RRSE) and the highest Pearson coefficient ( $\rho$ ). In the same way, the variable that correlates the best with the combined surge and wave parameters is the total (flow plus wave) force, using the IGN+Structures topography and bathymetry (Table 1). This is related with the fact that this digital elevation model includes thin flood walls that contribute to protection, and which can substantially modify the flow and wave fields over land.

160 **Table 2: Goodness of fit for the flow only, and flow plus wave, parameters. The best fits for flow-only parameters are indicated in green, and the best fits for flow plus wave parameters are indicated in blue.**

Variable	RMSE			$\rho$			RRSE		
	GEBCO	IGN	IGN + Structures	GEBCO	IGN	IGN + Structures	GEBCO	IGN	IGN + Structures
Water depth (h)	0.1595	0.1898	0.1495	0.8134	0.7344	0.8328	0.1009	0.1145	0.0902
Flow speed (v)	0.3586	0.2561	0.2234	0.1284	0.5387	0.6406	0.2268	0.1545	0.1347
Unit discharge ( $hv$ )	0.3352	0.2272	0.2120	0.2421	0.6558	0.6744	0.2120	0.1370	0.1278
Flow momentum flux ( $\rho hv^2$ )	0.3542	0.2540	0.1822	0.1314	0.5759	0.7622	0.2136	0.1532	0.1099
Significant wave height ( $H_{sig}$ )	0.2211	0.2030	0.1600	0.6432	0.6901	0.8066	0.1398	0.1224	0.0965
Total water depth ( $h + H_{sig}$ )	0.1767	0.2217	0.1522	0.7575	0.6404	0.8265	0.1117	0.1337	0.0918
Wave energy flux ( $E_f$ )	0.2649	0.2391	0.2307	0.5519	0.5851	0.6510	0.1676	0.1442	0.1391
Total force ( $\frac{E_f}{c_d} + \rho hv^2$ )	0.3307	0.2494	0.1499	0.2396	0.5888	0.8387	0.2092	0.1504	0.0904

#### 4 Discussion

165 The present paper considered the influence of flow-only variables ( $h, v, hv, \rho hv^2$ ), and combined flow-wave parameters ( $hsig, h + H_{sig}, E_f, \frac{E_f}{c_d} + \rho hv^2$ ). Flow depth and total (flow plus wave) force produce the best fits with analytical functions. Goodness of fit to damage curves improve with quality of the topographic data used (Table 1). However, when applying damage curves in practice, it is important to base predictions off a similar model setup to that used when calculating the damage curves in the first place (Brussee et al., 2021). For example, if damage curves are built using coarse topography that neglects the presence of thin seawalls (i.e. sheetpile/cantilever walls, or T- or L- walls), then the buildings protected by these walls  
 170 might experience more intense hydrodynamic conditions in the simulation than if the walls had been present in the simulation. Since the actual recorded damage does not depend on the model used to calculate the hydrodynamic forcing conditions, damage



175 curves developed using the coarse resolution topography will be shifted to the right relative to damage curves generated with  
the thin floodwalls present. If these damage curves generated using a coarse resolution simulation are then applied for damage  
prediction by an external user who applies a high resolution simulation that resolves floodwalls, the reduced forcing (due to  
the presence of these floodwalls) will generate a non-conservative result (too little damage), because the damage curves had  
180 been generated using forcing data from a simulation where the floodwalls had not been present. Therefore, when damage  
curves are reported in the literature, it is important to quantify how these vary with the topography used in the simulations on  
which the damage curves are based. However, in the current paper, Figure 7 shows that damage curves do not vary consistently  
leftward or rightward as topographic data are improved. This is because the response of forcing to the presence of these walls  
185 is more complex than simply reducing wave height. If not overflowed, walls reduce damage greatly. However, water depth  
can be exacerbated in front of walls, and flow can be channelled and intensified along walls, all increasing hydrodynamic  
forcing in some locations, preventing a simple relation between topographic resolution and damage curve robustness.

185 In addition to the general sensitivity of damage curves to topographic data quality, the damage curves displayed in Figure 7  
do not consider certain physical wave-driven phenomena such as wave overtopping of structures (Lashley et al., 2020a) or  
infragravity waves generated by waves breaking in shallow water (Roeber and Bricker, 2015). For instance Lashley et al.  
(2019) discussed the importance of dike overtopping due to infragravity waves on nearshore developments that can induce  
wave-driven coastal inundation. The wave model used here, SWAN, does not include infragravity waves, nor does the  
190 combined Delft3D/SWAN flow/wave model simulate wave overtopping of dikes, possibly leading to an underestimation of  
the hydrodynamic forces on buildings, which would affect the resulting damage functions. However, consideration of wave  
overtopping and infragravity effects requires either phase-resolving wave simulations or empirical relations specific to the  
local topography (Lashley et al., 2020b), though this is beyond the scope of the current study, and is similarly neglected by  
most other large-scale inundation studies (i.e., Sebastian et al, 2014; Kress et al., 2016; Kowaleski et al., 2020). Nonetheless,  
the effect of infragravity oscillations and wave overtopping on resulting damage is an important item for future research.

## 195 **5 Conclusions**

Using insurance claims to build damage curves from the structures located in La Rochelle and surroundings provides valuable  
information on the future damages that can be expected from an extratropical storm strike on the French Atlantic coast. In the  
present study, the best correlation between the damage ratio and the hydrodynamic variables are the flow depth and the total  
(flow plus wave) force for the aforementioned flow-only and flow-plus-wave variables respectively.

200

The uncertainty and variability within this methodology can be explained by two factors: 1) the hydrodynamic modelling, and  
consequently, uncertainty in the hydrodynamic variables, and 2) uncertainty in the claims data. Regarding the first point, there  
is a trend that indicates that better topography/bathymetry data gives hydrodynamic variables that correlate better with the



205 damage ratio. The explanation of this is basically because higher resolution data brings generally more accurate results of the  
real flood conditions (Luppichini et al., 2019 and Ettritcha et al., 2018). Damage curves developed with a better representation  
of the topography (IGN + structures) improve the accuracy indicators (Table 2), though scatter in the data itself (Figures A1,  
A2 or A3) is large for all topographies. The second point, deals with the quality of the damage ratio data. It is well identified  
that claims are subject to fraud and information distortion. Also variables related with the vulnerability of the assets like the  
construction characteristics, the materials, the quality and the age of the structures (Paprotny et al., 2021) play an important  
210 role in whether for a particular hydrodynamic variable value damage occurs or not. This adds a degree of complexity to the  
analysis

In addition to the sensitivity of results to resolution of the topographic and bathymetric data, the inclusion of thin flood walls  
via a land survey carried out by the authors also had a significant effect on the damage functions generated. This is important  
215 to note, as thin steel or concrete structures like flood walls at typically only a few 10's of centimetres thick, and so do not  
appear in digital elevation models. The effect of these thin structures on the resulting damage functions shows the importance  
of locally sourcing elevation data for the thin structures that are present, when conducting risk analyses for coastal regions,  
though it is imperative to keep in mind agreement between the simulations used for developing the damage relations in the  
first place, with those where the damage relations are applied for further risk analysis.

## 220 **Acknowledgements**

This work is funded by the AXA Joint Research Initiative (JRI) project INFRA: Integrated Flood Risk Assessment. A special  
acknowledgement to Adri Mourits from Deltares for the help provided with the Delft3d debugging and Christopher Lashley  
for the help during the field trip in Ile du Re and surrounding during August of 2020.

## **References**

- 225 Bricker J., Esteban M., Takagi H., Roeber V., “Economic feasibility of tidal stream and wave power in post-Fukushima Japan”,  
*Renewable Energy*, 114 pg32-45, 2017.
- Brussee, A.R., Bricker, J.D., De Bruijn, K.M., Verhoeven, G.F., Winsemius, H.C. and Jonkman, S.N., Impact of hydraulic  
230 model resolution and loss of life model modification on flood fatality risk estimation: Case study of the Bommelerwaard, The  
Netherlands. *Journal of Flood Risk Management*, p.e12713, 2021.



- 235 Büttner O., “The influence of topographic and mesh resolution in 2D hydrodynamic modelling for floodplains and urban areas”, EGU General Assembly Conference Abstracts, 2007.
- De Risi R., Goda K., Yasuda T., Mori N., “Is flow velocity important in tsunami empirical fragility modeling?”, *Earth-Science Reviews*, Volume 166, Pages 64-82, ISSN 0012-8252, 2017.
- 240 Deltares, “Delft3d user manual”, Version: 3.15, SVN Revision: 70333, 2021.
- Chauveau E., Chadenas C., Comentale B., Pottier P., Blanlœil A., Feuillet T., Mercier D., Pourinet L., Rollo N, Tillier I. and Trouillet B., *Xynthia: lessons learned from a catastrophe*, Environment, Nature and Landscape, <https://doi.org/10.4000/cybergeogeo.28032>, 2011.
- 245 Enghardt J., de Moel H., Huyck C., de Ruiter M., Aerts J. and Ward P., “Enhancement of large-scale flood risk assessments using building-material-based vulnerability curves for an object-based approach in urban and rural areas”, *Natural Hazards and Earth System Sciences*, 2019.
- 250 Ettritcha G., Hardya A., Bojangb L., Crossc D., Buntinga P. and Brewera P ., “Enhancing digital elevation models for hydraulic modelling using flood frequency detection”, *Remote Sensing of Environment*, 217, 506–522, 2018.
- GEBCO, The General Bathymetric Chart of the Oceans, available at: <https://www.gebco.net/>, 2020.
- 255 Hatzikyriakou A. and Lin N., *Assessing the Vulnerability of Structures and Residential Communities to Storm Surge: An Analysis of Flood Impact during Hurricane Sandy*, *Front. Built Environ*, 2018.
- Huizinga, J., De Moel, H. and Szewczyk, W., *Global flood depth-damage functions: Methodology and the database with guidelines*, EUR 28552 EN, Publications Office of the European Union, Luxembourg, ISBN 978-92-79-67781-6, doi:10.2760/16510, JRC105688, 2017.
- 260 Jansen, L., Korswagen, P. A., Bricker, J. D., Pasterkamp, S., de Bruijn, K. M., & Jonkman, S. N., Experimental determination of pressure coefficients for flood loading of walls of Dutch terraced houses. *Engineering Structures*, 216, 110647, 2020.
- 265 Kowaleski, A.M., Morss, R.E., Ahijevych, D. and Fossell, K.R., Using a WRF-ADCIRC ensemble and track clustering to investigate storm surge hazards and inundation scenarios associated with Hurricane Irma. *Weather and Forecasting*, 35(4), pp.1289-1315, 2020.



- 270 Kreibich H., Piroth K., Seifert I., Maiwald H., Kunert U., Schwarz J., Merz B. and Thieken A., “Is flow velocity a significant parameter in flood damage modelling?”, *Natural Hazards and Earth System Sciences*, 2009.
- Kress, M.E., Benimoff, A.I., Fritz, W.J., Thatcher, C.A., Blanton, B.O. and Dzedzits, E., Modeling and simulation of storm surge on Staten Island to understand inundation mitigation strategies. *Journal of Coastal Research*, (76), pp.149-161, 2016.
- 275 Lashley C., Bertin X., Roelvink D. and Arnaud G., “Contribution of Infragravity Waves to Run-up and Overwash in the Pertuis Breton Embayment (France)”, *Journal of Marine Science and Engineering*, 2019.
- Lashley, C.H., Bricker, J.D., van der Meer, J., Altomare, C. and Suzuki, T., Relative magnitude of infragravity waves at coastal dikes with shallow foreshores: a prediction tool. *Journal of Waterway, Port, Coastal, and Ocean Engineering*, 146(5), p.04020034, 2020a.
- 280 Lashley, C.H., Zanuttigh, B., Bricker, J.D., van der Meer, J., Altomare, C., Suzuki, T., Roeber, V. and Oosterlo, P., Benchmarking of numerical models for wave overtopping at dikes with shallow mildly sloping foreshores: Accuracy versus speed. *Environmental Modelling & Software*, 130, p.104740, 2020b.
- 285 Luppichini M., Favalli M., Isola I., Nannipieri L., Giannecchini R. and Bini M., “Influence of Topographic Resolution and Accuracy on Hydraulic Channel Flow Simulations: Case Study of the Versilia River (Italy)”, *Remote Sensing*, 2019.
- Muis S., Verlaan M., Winsemius H., Aerts J. and Ward P., “A global reanalysis of storm surges and extreme sea levels”, *Nature Communications* 7, 11969, 2016.
- 290 Paprotny D., Kreibich H., Morales-Nápoles O., Wagenaar D., Castellarin A., Carisi F., Bertin X., Merz B. and Schröter K., “A probabilistic approach to estimating residential losses from different flood types”, *Natural Hazards* 105:2569–2601, 2021.
- Pistrika A., Jonkman S., “Damage to residential buildings due to flooding of New Orleans after hurricane Katrina”, *Journal of Natural Hazards*. Vol. 54 pg; 413-434, 2010.
- 295 Postacchini M., Zitti G., Giordano E., Clementi F., Darvini G., Lenci S., “Flood impact on masonry buildings: The effect of flow characteristics and incidence angle”, *Journal of Fluids and Structures*, Volume 88, 2019.



- 300 Pregnolato M., Galasso C. and Parisi F., “A Compendium of Existing Vulnerability and Fragility Relationships for Flood: Preliminary Results”, 12th International Conference on Applications of Statistics and Probability in Civil Engineering, 2015.
- Reese S. and Ramsay D., “RiskScape: Flood fragility methodology”, Technical Report: WLG2010-45, 2010.
- 305 Roeber, V. and Bricker, J.D.. Destructive tsunami-like wave generated by surf beat over a coral reef during Typhoon Haiyan. *Nature communications*, 6(1), pp.1-9, 2015.
- Sebastian, A., Proft, J., Dietrich, J.C., Du, W., Bedient, P.B. and Dawson, C.N., Characterizing hurricane storm surge behavior in Galveston Bay using the SWAN+ ADCIRC model. *Coastal Engineering*, 88, pp.171-181, 2014.
- 310 Sihombing F. and Torbol M., “Analytical fragility curves of a structure subject to tsunami waves using smooth particle hydrodynamics”, *Smart Structures and Systems*, 2016.
- Slomp R., Kolen B., Bottema M. and Teun Terptsra, Learning from French Experiences with Storm Xynthia – Damages after  
315 A Flood”, *Learning from large flood events abroad*, 2010.
- Smith S., and Banke E.. “Variation of the sea surface drag coefficient with wind speed.” *Quarterly Journal of the Royal Meteorological Society* 101: 665–673, 1975.
- 320 Suppasri, A., Mas, E., Charvet, I., Gunasekera, R., Imai, K., Fukutani, Y., Abe, Y., Imamura, F., Building damage characteristics based on surveyed data and fragility curves of the 2011 great east Japan tsunami. *Nat. Hazards* 66 (2), 319–341, 2013.
- Tiggeloven T., de Moel H., Winsemius H., Eilander D., Erkens G., Gebremedhin E., Diaz-Loaiza A., Kuzma S., Luo T.,  
325 Iceland C., Bouwman A., van Huijstee J., Ligtoet W. and Ward P.,” Global-scale benefit–cost analysis of coastal flood adaptation to different flood risk drivers using structural measures”, *Natural Hazards and Earth System Sciences*, 2020.
- Tomiczek T., Kennedy A., Zhang Y., Owensby M., Hope M., Lin N., and Flory A., “Hurricane Damage Classification Methodology and Fragility Functions Derived from Hurricane Sandy’s Effects in Coastal New Jersey”, *Journal of Waterway  
330 Port Coastal and Ocean Engineering*, 2017.
- Tsubaki R., Bricker J., Ichii K. and Kawahara Y., “Development of fragility curves for railway embankment and ballast scour due to overtopping flood flow”, *Natural Hazards and Earth System Sciences*, 2016.



Appendix A

335 Whisker plots from which damage curves are developed are shown in Figures A1, A2, and A3. Digital Elevation Models are as described in Table 1. The damage curves of Figure 7 use the median values (red lines) from each of the figures in this appendix.

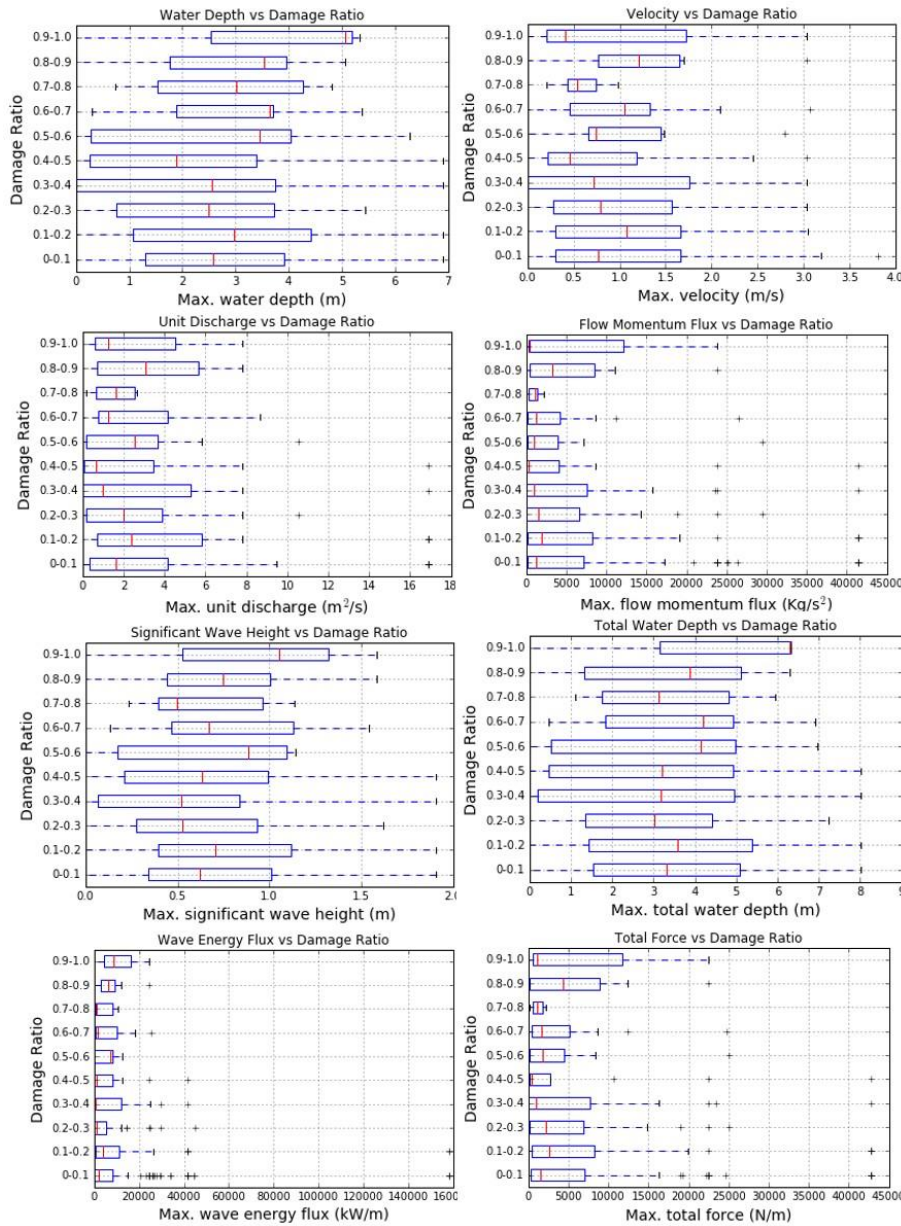
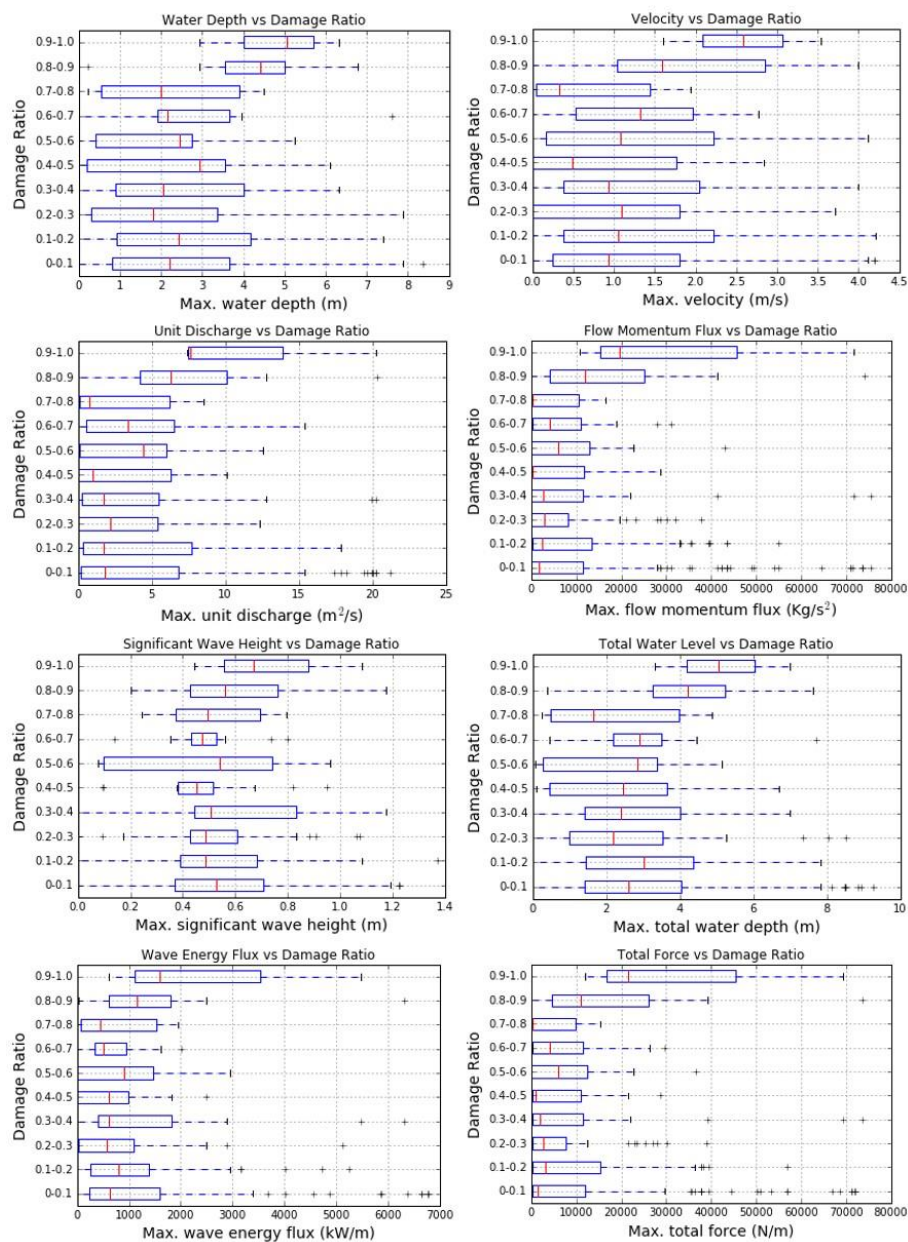


Figure A1: Box-Whisker plots for the variables ( $h, v, hv, hv^2, H_{sig}, h + H_{sig}, E_f, \frac{E_f}{C_g} + \rho hv^2$ ) with the GEBCO DEM.





340

Figure A2: Box-Whisker plots for the variables ( $h, v, hv, hv^2, H_{sig}, h + H_{sig}, E_f, \frac{E_f}{C_g} + \rho hv^2$ ) with the IGN DEM.

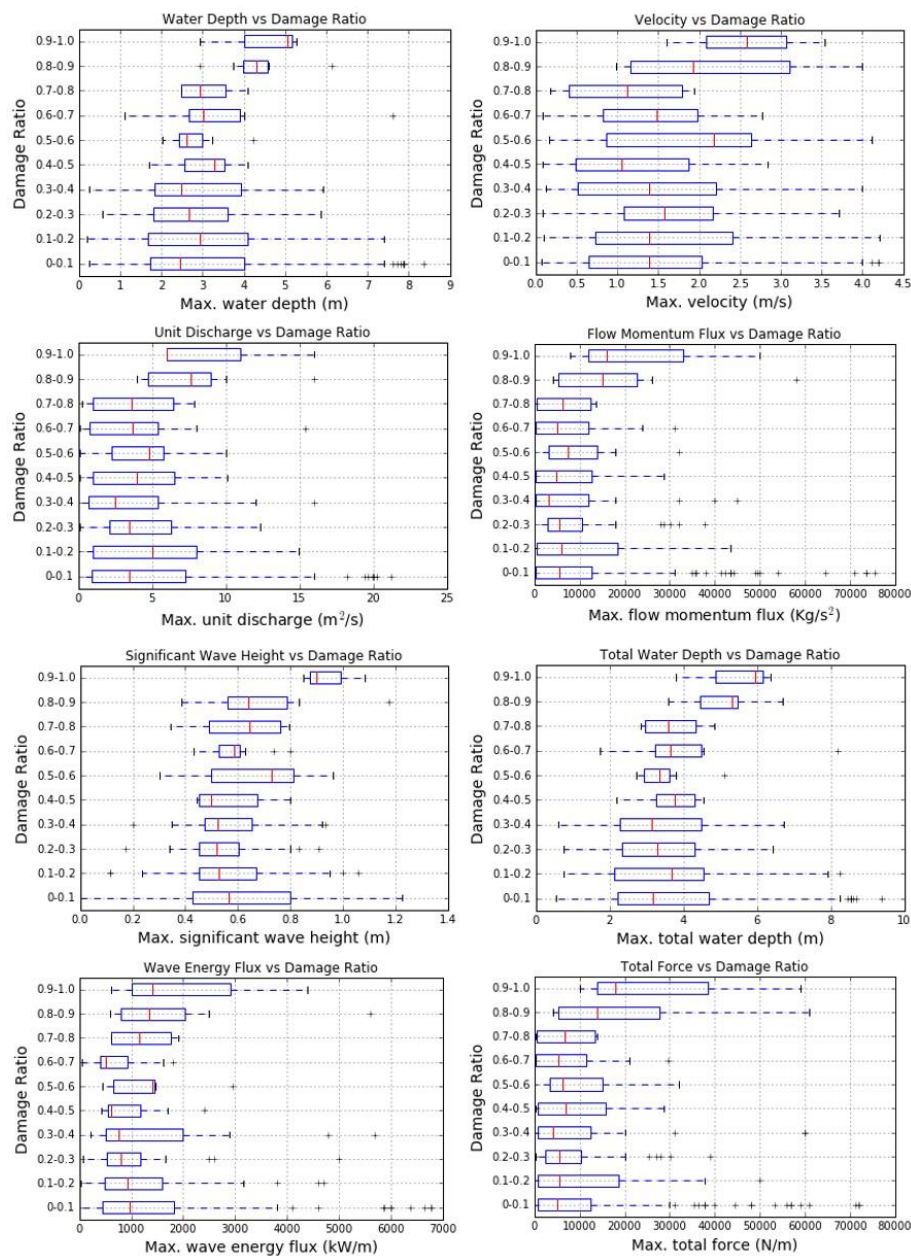


Figure A3: Box-Whisker plots for the variables ( $h, v, hv, hv^2, H_{stg}, h + H_{stg}, E_f, \frac{E_f}{C_g} + \rho hv^2$ ) with the IGN+Structures DEM.